Journal of Membrane Science 608 (2020) 118241

Contents lists available at ScienceDirect

Journal of Membrane Science

journal homepage: http://www.elsevier.com/locate/memsci

Polyarylene thioether sulfone/sulfonated sulfone nanofiltration membrane with enhancement of rejection and permeability via molecular design☆

Pengrui Jin [a], Shushan Yuan [a,*], Gang Zhang [b,*], Junyong Zhu [c], Junfeng Zheng [a], Patricia Luis [d], Bart Van der Bruggen [a,e]

[a] Department of Chemical Engineering, KU Leuven, Celestijnenlaan 200F, B-3001 Heverlee, Belgium
[b] Institute of Materials Science and Technology, Sichuan University, Chengdu 610064, PR China
[c] School of Chemical Engineering and Energy, Zhengzhou University, Zhengzhou 450001 PR China
[d] Materials & Process Engineering (iMMC-IMAP), UC Louvain, Place Sainte Barbe 2, 1348 Louvain-la-Neuve, Belgium
[e] Faculty of Engineering and the Built Environment, Tshwane University of Technology, Private Bag X680, Pretoria 0001, South Africa

ARTICLE INFO

Keywords:
Molecular design
Oxidization treatment
Improving performance
Dye desalination

ABSTRACT

Further improvement of nanofiltration is significantly hindered by the trade-off between the permeability and selectivity. This study proposes a new strategy of significantly improving performance by enhancing the effective membrane area, hydrophilicity, membrane porosity, negative charges of a membrane, and decreasing pore size through designing a new polyarylene thioether sulfone/sulfonated sulfone (PATS/SS) copolymer. Via copolymerization, thioether (-S-) and sulfonic groups were integrated in one polymer, endowing it with oxidizable properties, in combination with improved hydrophilicity, negative charges and membrane porosity. Nanofiltration membranes prepared from this copolymer are hydrophilic (contact angle: 69.1°) and negatively charged. After the -S- groups were altered to sulfone (–SO_2–) units by a simple oxidization treatment, both hydrophilicity (contact angle: 37.9°) and surface charge were enhanced, rendering improved antifouling properties. Furthermore, the solvent stability of oxidized membranes was significantly improved, maintaining the structure intact even in N-methyl-2-pyrrolidone (NMP) for 24 h. Most importantly, a simultaneous enhancement of rejection (by 85.2%) and permeability (by 105%) of the membrane was observed when applied in nanofiltration for water purification and dye desalination, significantly improving performance compared to currently reported membranes.

1. Introduction

Nanofiltration has attracted extensive research interest due to its low investment cost, high efficiency and green approach by simply applying a pressure gradient [1–3]. Conventional pressure driven nanofiltration membranes have a molecular weight cutoff range of 200–1000 Da and pore size of about 0.5–2.0 nm [4]. As the core part of a nanofiltration device, the selective membrane should have high membrane flux, sufficient rejection and excellent antifouling properties at the same time [2,5]. However, in practical applications, the rejection of a nanofiltration membrane usually increases by sacrificing membrane flux, and vice versa. As a result, the application of the membrane is primarily limited by its intrinsic trade-off between permeability and selectivity [6–8].

In order to overcome the trade-off between permeability and selectivity, many efforts have been made [6]. Biological membranes have both extremely high permeability and selectivity, which stimulated the development aquaporin membranes, but so far no reports have shown that aquaporin membranes are highly selective [9,10]. Block copolymers provide opportunities for the production of isoporous membranes (with pore size reduced to 1.5 nm, and still maintain high flux) by utilizing their ability to self-assemble to form a narrow pore size distribution [11,12]. However, block copolymers are expensive compared to traditional polymers for water purification membranes; the cost of block copolymers can be a significant barrier, limiting their use to high value, low volume separations. Inorganic materials (MOFs, MXenes, graphene-based materials, etc.) can provide an effective strategy for adjusting the pore size and shape of the selective membrane, and contribute to the narrow pore size distribution of a selective membrane, making the membrane highly permeable and selective [13–15]. According to the above reports, the mainstream strategy of present

* Corresponding authors.
E-mail addresses: shushan.yuan@kuleuven.be (S. Yuan), gangzhang@scu.edu.cn (G. Zhang).

https://doi.org/10.1016/j.memsci.2020.118241
Received 16 February 2020; Received in revised form 1 May 2020; Accepted 4 May 2020
Available online 6 May 2020

research is to increase the free volume of the membrane (increasing permeability) while simultaneously narrowing the size distribution of the free volume (increasing selectivity). Due to the complexity and high cost of adjusting the pore structure, this strategy is not suitable for industrial application. Therefore, it is necessary to develop cheap and efficient strategies to break through the trade-off between permeability and selectivity.

In nanofiltration, electrostatic repulsion, the dielectric effect and size exclusion are the main rejection mechanisms for anionic dyes [16–20]. Therefore, if the membrane exhibits strongly negative charge or a small and uniform pore size, it will contribute to improve the membrane selectivity for anionic dyes. Furthermore, the permeability is affected by the water-permeable area and the hydrophilicity of the selective membrane. The increase of the water-permeable area of the support membrane per unit area is beneficial to improve the permeability of the membrane [3]. For example, a film with crumpled texture has a larger surface area and a better permeability than a smooth film. Besides, improving the hydrophilicity can ensure that the membrane has a good antifouling ability, in order to avoid foulant adhesion/membrane pore blocking and to ensure high flux operation of the nanofiltration for dye solutions [2,21]. In addition, pore size and porosity also play a decisive role in improving the separation performance. However, to the best of our knowledge, breaking through the trade-off based on improving the membrane porosity electrical charge, the effective area, hydrophilicity and decreasing pore size at the same time has not been reported elsewhere. In addition, it has not been studied which materials and modification methods can be used to achieve this effect.

Polymer molecular designing is an emerging method to address membrane separation problems [22]. Sulfonated polymers are characterized by a good hydrophilicity, low contamination tendency, selective ion migration and chlorine resistance, which can be used to improve the membrane permeability [23]. Therefore, it is a good choice to introduce sulfonic groups into the nanofiltration membrane. However, a high sulfonation could lead to a decreased solvent resistance of a polymer, resulting in a deterioration of the selectivity of such sulfonated membrane in applications. Thioether groups (-S-) can be utilized to enhance the solvent resistance of a polymer by oxidization [24]. The -S- group in a poly(arylene sulfide sulfone) membrane can be oxidized to $–SO_2-$ by oxidation (with hydrogen peroxides, acetic acid, sulfuric acid), which can improve the molecular chain packing density, rigidity and interaction [24]. In addition, due to the dramatic increase of oxygen-containing groups, the pore sizes of membrane are greatly decreased, which favor a higher selectivity. Therefore, it is speculated that if the sulfonic group and the $–SO_2-$ bond can be introduced into the same molecular chain, the purpose of significantly improving performance can be achieved, however, it has never been explored.

In this study, a new high-performance membrane was developed by designing a polymer PATS/SS with sulfonic and $–SO_2-$ groups. The functionalized membranes are extensively characterized to confirm the successful molecular design of PATS/SS and to evaluate its effect on the nanofiltration properties. The aim of this study is not only to provide a new candidate membrane for water purification and dye desalination, but also to develop an efficient molecular design method in order to enhance the potential of membrane applications.

2. Experiment

2.1. Chemicals and materials

Sulfuric acid, anhydrous potassium carbonate, fuming sulfuric acid (30% SO_3) (all from Chengdu Ke Long Co. Ltd, China) were used as received. 4,4′-thiodibenzenethiol (TDB, 99.5%) was procured from ZheJiang ShouErFu Chemical Industry Company (China). 4, 4′-dichlorodiphenyl sulfone (DCDPS, AR) was obtained from JiangXi Jinhai New energy technology Limited company (China). The disodium 3, 3′-disulfonate-4, 4′-dichlorodiphenylsulfone (SDCDPS) monomer used in this study was synthesized based on a similar method as reported earlier [25,26]. Polyarylene thioether sulfone/sulfonated sulfone (PATS/SS) with sulfonation degree of 20, 30 and 40 mol% was synthesized by aromatic nucleophilic substitution at atmospheric pressure. N-methyl-2--pyrrolidone (NMP, 99%) from Sigma-Aldrich and deionized water were used as the solvent and coagulant for membrane fabrication. Novatexx 2471 non-woven (thickness 0.18 mm) was provided by Freudenberg Performance Materials. A mixed solution including hydrochloride peroxide (H_2O_2, 30% by weight), sulfuric acid (H_2SO_4, 97–98%), acetic acid (CH_3COOH, 99%) from Sigma-Aldrich was used as the oxidant. Dyes listed in Table S1 including Direct Red 80 (DR80), Direct Red 23 (DR23), and Reactive Orange 16 (RO16) from Sigma-Aldrich, were utilized to measure the molecular weight cut-off of the membranes. Sodium sulfate (Na_2SO_4, 99%) from Sigma-Aldrich was used to test salt permeation.

2.2. Preparation of monomers and copolymers

2.2.1. Synthesis of disodium 3, 3′-disulfonate-4, 4′-dichlorodiphenylsulfone (SDCDPS)

As shown in Fig. 1a and b, 0.3 mol DCDPS was added into a three-neck flask that was equipped with a mechanical stirrer and allihn condenser. Then 140 ml 30% fuming sulfuric acid was added. Afterwards, the mixture was heated up to 110 °C, and kept for about 6 h. Then the reaction mixture was poured into ice-water and NaCl was added into the solution with stirring. The white precipitate was collected, and dissolved with deionized water, neutralized with NaOH until the pH value of the solution was about 8–9. Then the solution was salted out with NaCl and filtrated. The precipitate was collected, and the solid was dried at 105 °C. The crude product was then recrystallized with the mixture of isopropyl alcohol and water to produce a white needle-like crystal. The crystal was dried at 90 °C under vacuum to yield SDCDPS 115.6 g (product yield: 78.6%).

2.2.2. Synthesis of polyarylene thioether sulfone/sulfonated sulfone copolymers (PATS/SS)s

The polyarylene thioether sulfone/sulfonated sulfone copolymers (PATS/SS)s with different amount of SDCDPS were synthesized via an aromatic nucleophilic substitution polymerization of 4,4′-thiodibenzenethiol (TDB) and various ratios of disulfonated monomers (SDCDPS) to non-sulfonated monomers (DCDPS) in N-methyl-2-pyrrolidone (NMP)/toluene (as shown in Fig. 1c). TDB (25 g), potassium carbonate (33.1g), DCDPS (23 g), SDCDPS (9.8 g), toluene (20 ml) and NMP (120 ml) was added into a three-necked round bottom flask. Then the reaction mixture was heated to 150–160 °C to remove the by-product water. Afterwards, a reaction temperature of 180–190 °C was applied for 8 h. During this procedure, the reaction solution became more and more viscous. After 8 h, the polymerization mixture was poured into water with stirring to precipitate gray fibrous solids, then the crude product was further acidified with hydrochloric acid and washed with hot water. After pulverizing the fibrous solids into powder, it was washed by deionized water and ethanol. After repeating the washing procedure 3 times, the copolymers were finally obtained. These were dried in a vacuum oven for 20 h at 105 °C; they were labeled as PATS/SS-20%, 20%represents sulfonation (Yield: 97.6%, Fig. S1).

With a similar procedure, PATS/SS-30% and PATS/SS-40% were prepared by adjusting the content of DCDPS and SDCDPS.

2.3. Membrane preparation

2.3.1. Membranes were prepared via nonsolvent induced phase inversion

As shown in Fig. 1a, dope solutions with PATS/SS concentration of 16.0, 18.0 and 20.0 wt% were prepared by dissolving 1.6, 1.8 and 2.0 g of PATS/SS materials in 8.4, 8.2 and 8.0 g of NMP, respectively, at room temperature for over 24 h. Before casting the PATS/SS membrane, the dope solution was centrifuged for 10 min at 4000 rmp to remove air

bubbles. The denotation 'PATS/SS (x/y)' represents a PATS/SS membrane prepared from a dope solution with sulfonation degree of x% and a PATS/SS dope solution concentration of y%. The polymer solutions were subsequently cast onto the surface of the non-woven fabric using a casting knife with a thickness of 200 μm at room temperature (Fig. S2). The non-woven fabric was then immediately immersed in a deionized water bath for phase separation. After the PATS/SS membrane was formed, it was kept immersed in deionized water to remove residual NMP.

2.3.2. Oxidization of membranes

The obtained PATS/SS membranes were immersed in an oxidizing solution at room temperature; the oxidizing liquid was composed of 10 vol% hydrogen peroxide (30%), 87 vol% acetic acid and 3 vol% concentrated sulfuric acid (98%). In order to completely oxidize the PATS/SS membrane, the oxidization time was selected to be 12 h. The oxidation principle is shown in Fig. 1d. After that, the oxidized membranes were transferred in to deionized water for 1 h to remove the residual oxidizing solvent; they were kept in deionized water for further testing. The oxidized membranes were coded as 'O PATS/SS (x/y)'. Fig. S2 shows the fabrication of the PATS/SS membrane and the oxidation-treatment process.

2.4. Characterization methods

Fourier transform infrared (FT-IR) and ^{1}H NMR were used to confirm the successful preparation of S-PASS copolymers. Fourier transform infrared (FT-IR) spectra of the samples were recorded on a Nicolet NEXUS 670 spectrophotometer. The samples of polymer were prepared in the pellet form by mixing the dry powder material with KBr. ^{1}H NMR

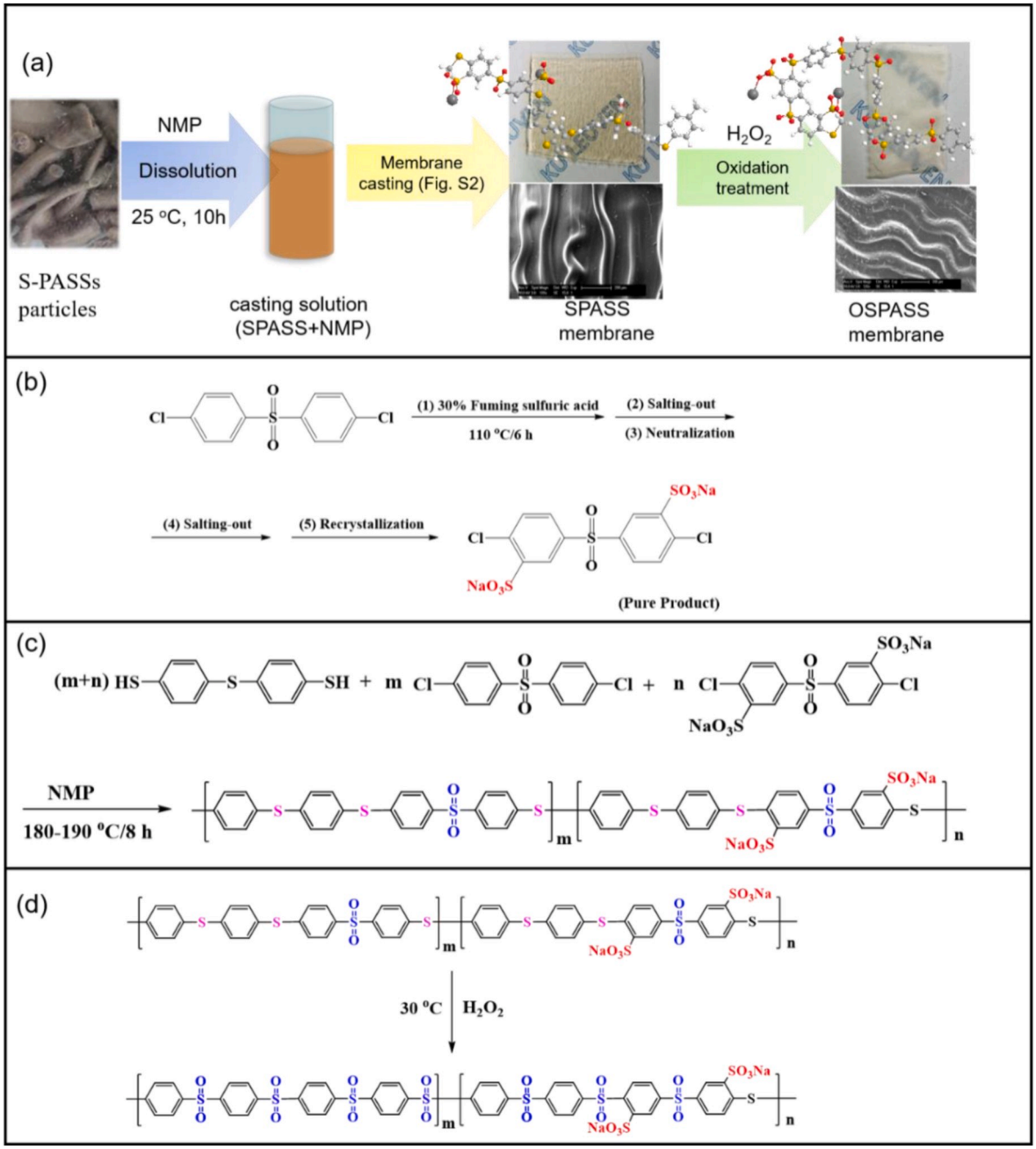

Fig. 1. Schematic overview of preparation of pristine and oxidized PATS/SS membrane: (a) The process of preparation of PATS/SS and oxidized PATS/SS membrane; (b) synthesis route of 3, 3′-disulfonate-4, 4′-dichlorodiphenylsulfone (SDCDPS); (c) synthesis; (d) oxidation treatment.

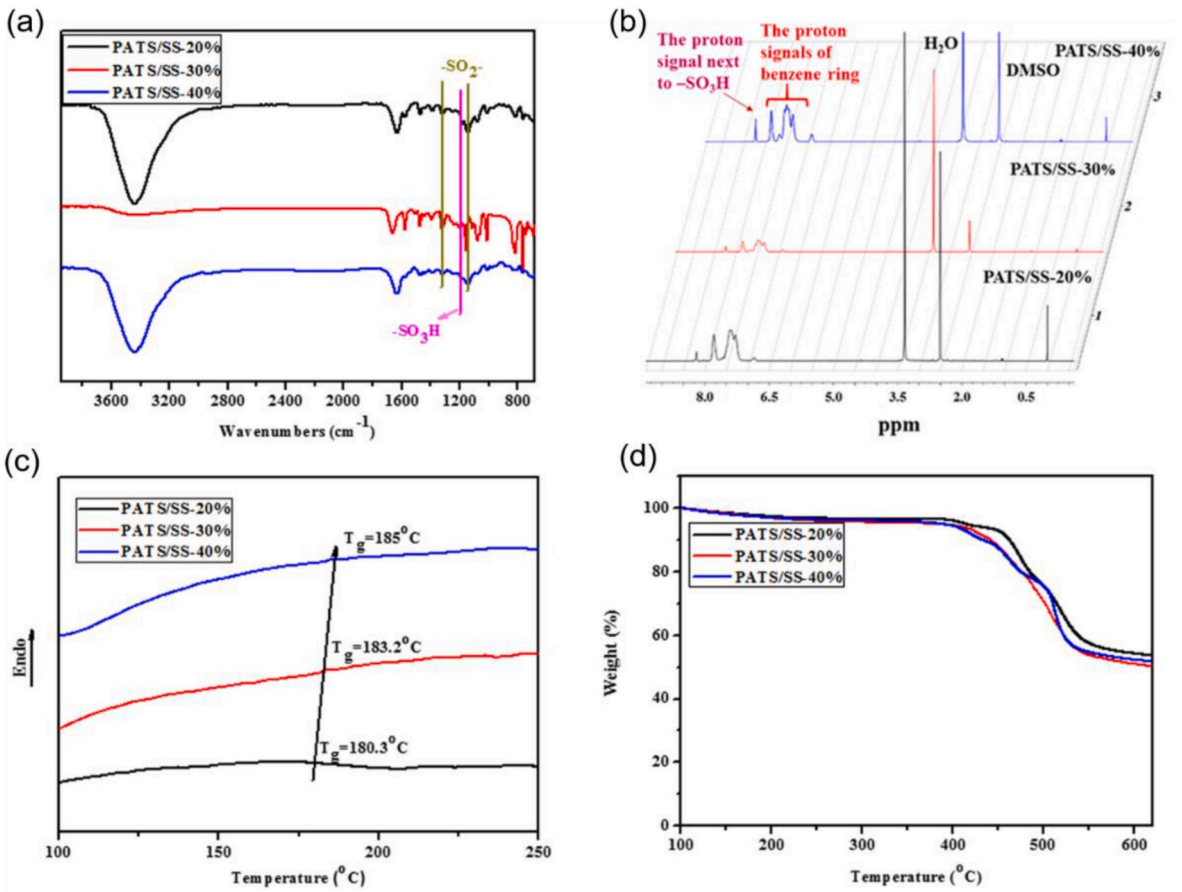

Fig. 2. (a) The FT-IR spectra of copolymers PATS/SS-(20%–40%); (b) The 1H NMR spectra of copolymers (20%–40%)-PATS/SS; (c) The DSC curves of PATS/SS-(20%–40%) at a heating rate of 10 °C/min in N2; (d) The TGA curves of PATS/SS-(20%–40%) at a heating rate.

spectra were recorded on a 400 MHz Bruker spectrometer using deuterated dimethyl sulfoxide (DMSO-d_6) as solvent and tetramethylsilane (TMS) as internal standard. Thermal analysis of these samples was performed by differential scanning calorimetry (DSC) and thermogravimetric analysis (TGA). DSC measurements were determined by a NETZSCH DSC 200 PC thermal analysis instrument. The heating rate for the TGA Q500 V6.4 Build 193 thermal analysis instrument. The heating rate for the TGA measurements was 10 °C/min under N_2 atmosphere.

In addition, the chemical changes of the oxidation reaction were recorded by a NEXUS670 Fourier transform infrared (FT-IR) spectrometer and Krais ULFRA x-ray photoelectron spectroscopy (XPS). The surface and cross-section morphologies of PATS/SS and OPATS/SS membranes were observed by field emission scanning electron microscopy (SEM, Netherlands). The samples were mechanically broken and dried in liquid nitrogen and then the cross-section was observed. A Dimension 3100 Atomic force microscopy (AFM, Bruker USA) was utilized to observe the surface roughness of the prepared membranes under ambient conditions in tapping mode with a scanning area of 2 × 2 μm^2 and 5 × 5 μm^2. A contact angle goniometer (OCA20, Dataphysics Instruments, Germany) was utilized to observe the hydrophilicity changes of these membranes before and after oxidization with a 3 μL water droplet. Each reported contact angle represents an average of five measurements taken at random positions on the membranes surface to minimize experimental errors. The zeta-potential was analyzed using a Zeta-potential & Particle size Analyzer Mastersizer NaNoZS.

2.5. Membrane performance

2.5.1. Evaluation of membrane separation performance

The separation performance (water flux, salt retention, and dye retention) of PATS/SS and OPATS/SS membranes was evaluated using a stainless-steel dead-end apparatus (HP4750) with an effective permeation membrane area of 14.6 cm^2. The nanofiltration equipment was continuously stirred at 500 rpm to minimize concentration polarization at 6 bar and room temperature. The water permeability (L m^{-2} h^{-1} bar^{-1}) was calculated by the following equation:

water permeability (L m^{-2} h^{-1} bar^{-1}) was calculated by the following equation:

$$WP = \frac{V}{A \cdot \Delta t \cdot P} \quad (1)$$

where V is the volume of the permeate (L), Δt is the operation time (h), the effective area A of the membrane (14.6 cm^2), P is the applied pressure.

PEG molecules with different molecular weights (200, 400, 600, 1000, 1500 and 3000 Da) were used as the solutes in aqueous solutions to obtain the molecular weight cut off (MWCO, molecular weight of solution with 90% rejection) and mean effective pore size as described in a previous method [27]. The PEG, salt and dye rejection (R, %) were calculated according to the following equation:

$$R = 1 - C_P / C_f \quad (2)$$

where C_f and C_p (g L^{-1}) are the solute concentration in the feed and permeate, respectively. The concentration of dye in the feed (500 ppm) and permeate were measured with a UV-spectrophotometer (Shimadzu,

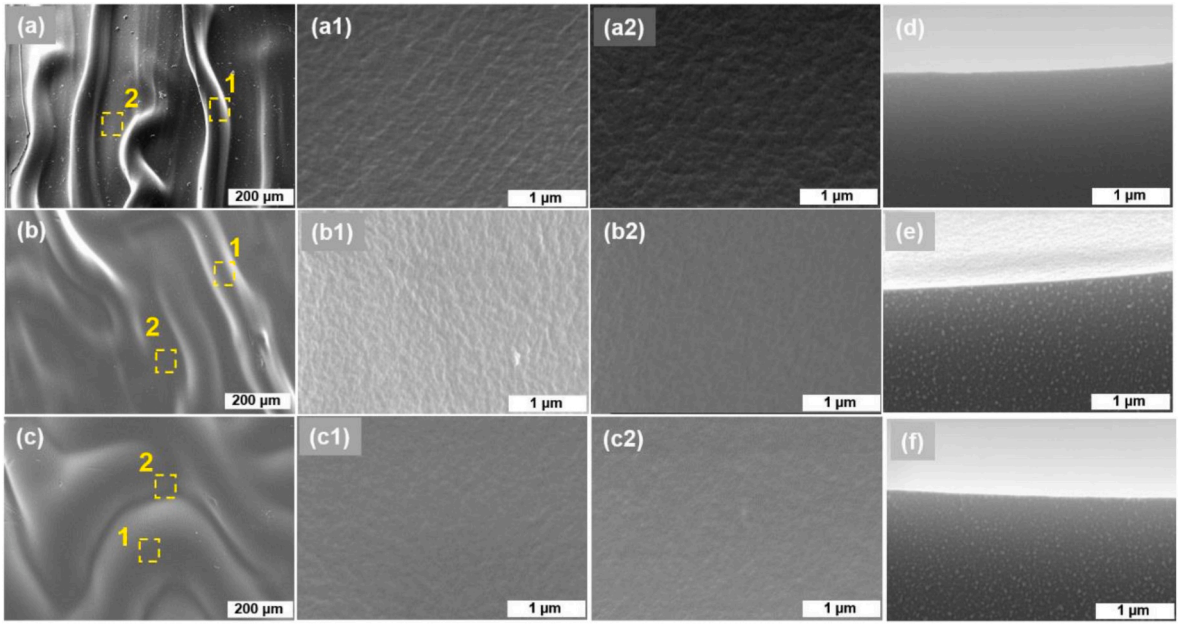

Fig. 3. (a-a2, d) SEM surface and cross-section images of PATS/SS (30/16) membrane, (b-b2, e) PATS/SS (30/18) membrane, and (c-c2, f) PATS/SS (30/20) membrane.

Japan). The concentration of salt in the feed (Na_2SO_4, 1.0 g L^{-1}) and permeate were measured by a conductivity meter (Thermo Scientific Orion Star A212). The concentration of PEG molecular was examined using a UV–visible absorption spectrophotometer at 535 nm with $BaCl_2$ and I_2/KI solutions as chromogenic reagents [28].

To measure the porosity of membrane substrates, wet membranes were taken out from the water bath followed by careful and quick removal of excess water on the surface by tissue paper. The wet membrane was then weighed (m_1, in g), freeze dried overnight, and re-weighed (m_2, in g). Subsequently, the absorbed water is calculated as m_1-m_2, and the dry weight of the membrane is m_2. The overall porosity was then obtained as follows:

$$\varepsilon = \frac{(m_1 - m_2)/\rho_w}{(m_1 - m_2)/\rho_w + m_2/\rho_P} \quad (3)$$

where ρ_w and ρ_P are the densities of water and polymer, respectively.

2.5.2. Solvent resistance performance after modification

In order to know the stability of PATS/SS and OPATS/SS membranes, they were immersed in NMP for 24 h.

3. Results and discussion

3.1. Synthesis of copolymers of PATS/SS-(20%–40%)

In order to achieve the molecular design of copolymers containing both sulfonic groups and -S- bonds, SDCDPS monomers containing a sulfonic group and TDB monomer containing an -S- bond were used. The polymerization reaction between TDB, DCDPS and SDCDPS monomers was carried out with a nucleophilic substitution method. K_2CO_3 was used as alkali to neutralization the active hydrogen of the TDB. The reaction temperature was first heated to 150–160 °C to form the organic salt and remove the by-product water, which was beneficial for the reaction of nucleophilic substitution reaction. After that, the reaction temperature was raised up to 180–190 °C to further enlarge the polymer's viscosity. Table S2 describes the intrinsic viscosities (η_{int}) of the copolymers.

The chemical structure of the prepared copolymers was characterized with FT-IR and ^{1}H NMR. As shown in Fig. 2a, from the difference between the FT-IR spectra, it can be obviously observed that the symmetric and asymmetric vibrations of the sulfonic group (-SO_3H) appearing near 1195 cm^{-1} enhanced with increasing the content of SDCDPS. And the absorption peaks around 1320 cm^{-1}, 1150 cm^{-1} and 1070 cm^{-1} were ascribed to the absorption peaks of –SO_2- and -S- unit, respectively. These peaks indicate that the copolymers containing sulfonic groups and -S- units were successfully synthesized. The composition of the polymer was further confirmed by H NMR. As shown in Fig. 2b, with increasing ratio of SDCDPS monomers, the proton signals around 8.3 ppm corresponding to sulfonic groups become more intense. Simultaneously, the signals attributed to the proton close to the -S- group became much smaller with decreasing ratio of DCDPS. In combination with the data of FT-IR, it is safe to conclude that the copolymers with integration of sulfonic groups and -S- units were synthesized as described in Fig. 1c. In addition, the thermal performance of copolymers PATS/SS-(20%–40%) was tested by DSC (Fig. 2c) and TGA (Fig. 2d).

The T_g values of PATS/SS-(20%–40%) were in the range of 180.3 and 185 °C, (as depicted in Fig. 2c). Increasing the content of SDCDPS increased the T_g of the copolymer, whereby the copolymer PATS/SS-40% showed the highest T_g value (185 °C) among this series. The reason could be that with the addition of monomer SDCDPS containing sulfonic group, the hydrogen bond density substantially increased; the interaction force between the polymer molecules was therefore enhanced, so the glass transition temperature of the copolymers showed an increasing trend with a higher copolymerization ratio of SDCDPS.

Fig. 2d shows the thermal degradation curves of PATS/SS-(20%–40%) in nitrogen atmosphere. The initial degradation temperatures (T5%) of PATS/SS-(20%–40%) were in the range of 382.3–413 °C, far above their T_g. The char yield of PATS/SS-(20%–40%) at 620 °C in nitrogen atmosphere was in the range of 44.8–53.6%. Based on the above results, it was concluded that the increase of the sulfonic groups ratio in polymer chain does not sacrifice the thermal performance of the copolymer.

3.2. PATS/SS membranes and the oxidized membranes

As shown in Fig. 3a–c, the membrane has an unconventional wave structure consisting of peaks and valleys (micron size). More specifically, the distance between two neighboring peaks or valleys is around

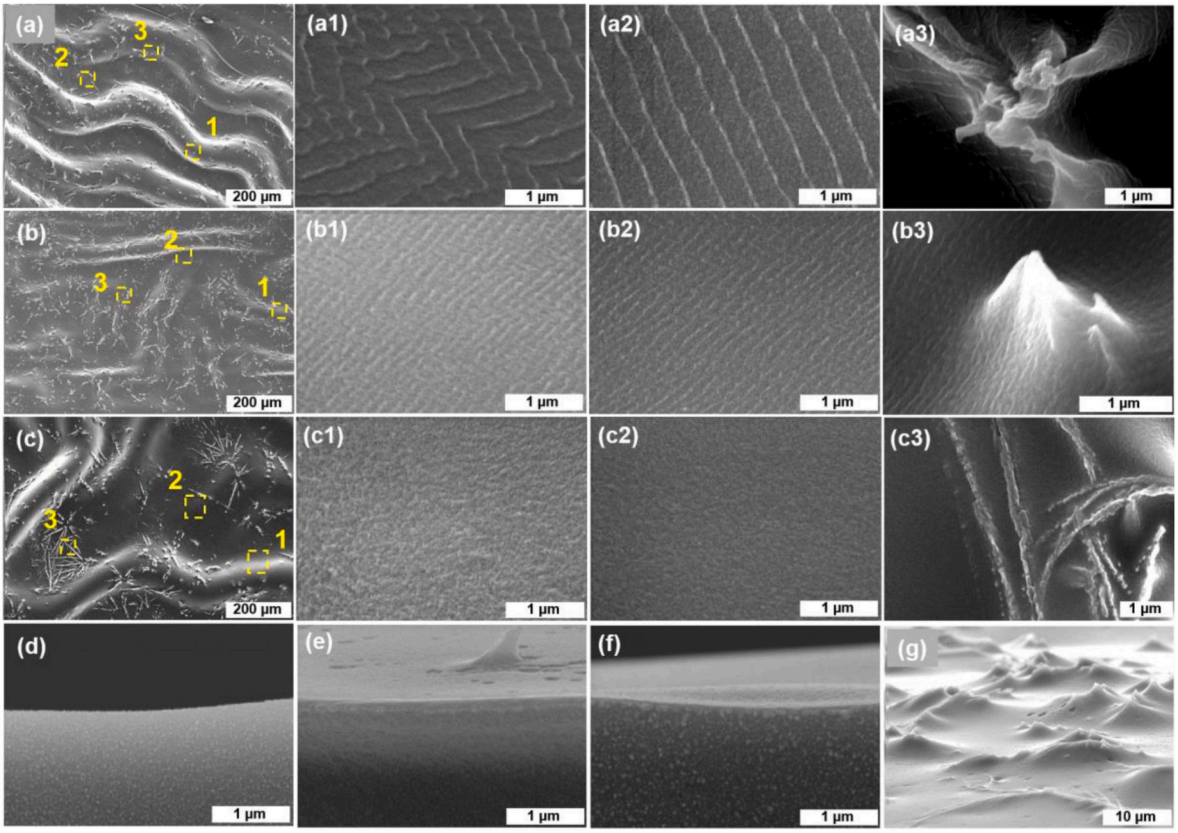

Fig. 4. SEM surface and cross-section images of oxidized membranes: (a-a3, d) OPATS/SS (30/16) membrane, (b-b3, e, g) OPATS/SS (30/18) membrane, and (c-c3, f) OPATS/SS (30/20) membrane.

150 μm. In addition, the wave structure gradually becomes flat with increasing concentration of the PATS/SS dope solution, implying that the formation of wave structures is due to the low concentration and low viscosity of the dope solution. The wave structure formed by surface collapse may be caused by gravity. The nonsolvent induced phase inversion first occurs in the surface layer. When the viscosity of the casting film under the surface layer is low, the instability of casting film (similar collapse) may occur under the action of gravity-driven convection, resulting in the appearance of a wave structure. The high-concentration and high-viscosity dope solution is more difficult to flow, and the impact of collapse caused by gravity becomes smaller [29,30]. There are also studies that suggest that these waves are caused by a combination of the stress caused by the contraction of the hard surface layer due to the solvent away, and the fact that the solvent-rich material underneath is still soft [31,32]. The cross-section morphology is presented in Fig. 3d–f and Fig. S6. The height of the casting knife was adjusted to 200 μm to all the substrate, after phase inversion, the thickness of these membrane obtained was in the range of 9–30 μm. The membrane thickness is uneven due to the presence of a wavy structure (the peaks are thicker, and the valleys are thinner). These copolymer membranes have a symmetric and sponge-like structure, which is uncommon to membranes synthesized by nonsolvent induced phase inversion as these have a typical asymmetric configuration with a thin surface layer on a porous carrier consisting of finger-like microporous structures [24]. Combined with the high permeability (see 3.3.2.), the measured high porosity (Table S3) and insights from the literature (sulfonated membranes tend to form sponge-like structure), it can be proven that the sulfonated membranes have a sponge-like structure [33–37]. During the phase inversion, several pathways may occur in the dope solution, which can be explained by ternary diagrams [38,39]. Based on the ternary diagram, adding sulphonated material would cause delayed demixing which results in the sponge-like PATS/SS substrate without macrovoid formation due to the hydrophilic nature of sulfonic groups [27,36]. Obviously, the presence of sulfonic acid groups can hinder the formation of macrovoids. Thus, instantaneous demixing occurs in non-sulfonated samples, resulting in macrovoid structures. The formation of macrovoids can be associated with many factors (solubility, coagulants, rheological properties and kinetics) [40–42]. This structural difference is mainly due to the presence of hydrophilic sulfonic groups, which are prone to form bonds with water. The much greater affinity of the sulfonated materials to water (non-solvent) leads to a longer time for the solvent and non-solvent exchange. This structural difference is mainly due to the delayed demixing induced by the hydrophilic nature of sulfonic groups, which would reduce macrovoid formation in a PATS/SS dense membrane (with nano level sponge-like structure) [27,43]. This kind of macrovoid-free membrane can be very stable under high pressure, which is beneficial for its application as a nanofiltration membrane.

As mentioned before, the -S- group can be oxidized to $–SO_2-$ by an oxidizing solution, which improves the solvent resistance of the membrane, negative charge and decreases the effective pore sizes. Interestingly, after the oxidation treatment of PATS/SS membrane, many volcanic structures appeared on the surface of the membrane (Fig. 4a3, b3, c3). In addition, a regular array of nano-sized triangular stripes was present at the bottom of the valleys and at the top of the peaks (Fig. 4a1, a2, b1 and b2). According to the scale bar in SEM results (Fig. 4), the size can be estimated. The width of nano-sized triangular stripes is about 60 nm. This is mainly attributed to swelling of the PATS/SS membrane in acidic solution [24]. During the oxidation process, acetic acid can make a PATS/SS membrane swell and invade the membrane body, which provides a channel for H_2O_2 molecules to enter the PATS/SS membrane. The H_2O_2 molecule can react with the -S- bond on the PATS/SS molecular chain, resulting in reconfiguration of the molecular chain. Finally, under the relaxation effect of swelling and reconfiguration of

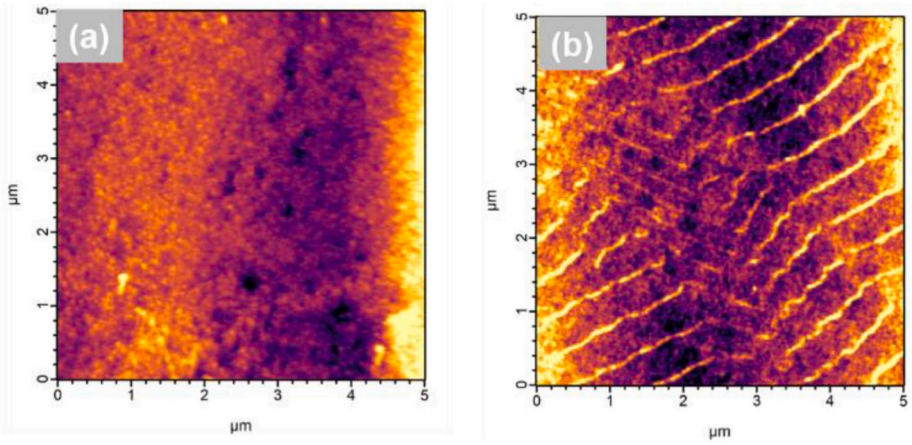

Fig. 5. AFM images of membrane surface: (a) PATS/SS (30/16); and (b) OPATS/SS (30/16).

Table 1
AFM surface roughness of pristine and oxidized PATS/SS membrane: Ra (average roughness), Rrms (root mean square roughness), and Rm (maximum vertical difference between the highest and lowest points).

Membrane	R_a (nm)	R_{rms} (nm)	R_m (nm)
PATS/SS (30/16)	3.450	4.341	34.639
OPATS/SS (30/16)	4.946	6.439	67.829
PATS/SS (30/18)	2.103	2.587	15.981
OPATS/SS (30/18)	2.650	3.339	24.369
PATS/SS (30/20)	1.393	1.754	15.135
OPATS/SS (30/20)	1.859	2.381	21.684

molecular reactions, micro level volcanic structures and nano level triangular waves crumpled appear on the surface of OPATS/SS membrane. This generates additional effective surface area, which is expected to enhance the membrane permeance [3,44]. Fig. 4g shows that the OPATS/SS membrane surface is constructed with micro level volcanic projections, which is in accordance with the results observed in Fig. 4a3, b3, c3. There is no significant difference between the original and oxidized PATS/SS membrane in cross sections, and the cross sections of both are very dense (Fig. 3d, e, f and 4(d, e, f)).

Comparing Figs. 3 and 4, the oxidation treatment had no obvious effect on the waves, but the valleys and peaks of the wave showed nano-sized triangular strips. The surface morphology and roughness parameters of the nano-sized triangular stripes were further explored by AFM, as shown in Fig. 5a and b. The surface roughness values of the membrane on 5 × 5 µm^2 scans are summarized in Table 1. As expressed by the roughness values (Table 1), the pristine PATS/SS membranes have a smoother surface with R_a = 3.450–1.393 nm, and R_{rms} = 4.341–1.754 nm than oxidized PATS/SS membranes (with R_a = 4.946–1.859 nm, and R_{rms} = 6.493–2.381 nm). After the oxidation treatment, the overall increased value in R_a and R_{rms} indicates that the oxidation reaction increases the membrane surface roughness, thus increasing the effective permeable area of the membrane surface, which is highly consistent with the SEM results discussed previously. In addition, with an increase of the concentration in the casting solution, the decrease in surface roughness confirms the formation of a denser, stronger membrane

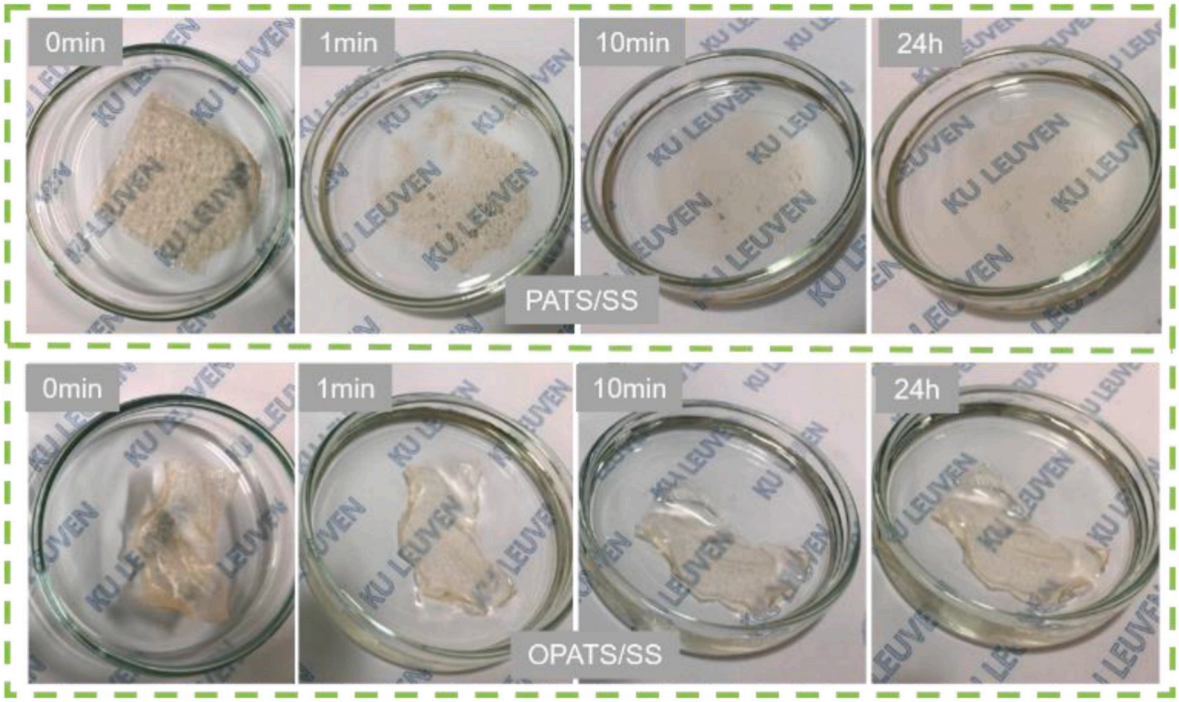

Fig. 6. PATS/SS membrane (first line) and OPATS/SS membrane (second line) after exposure to NMP for 24 h.

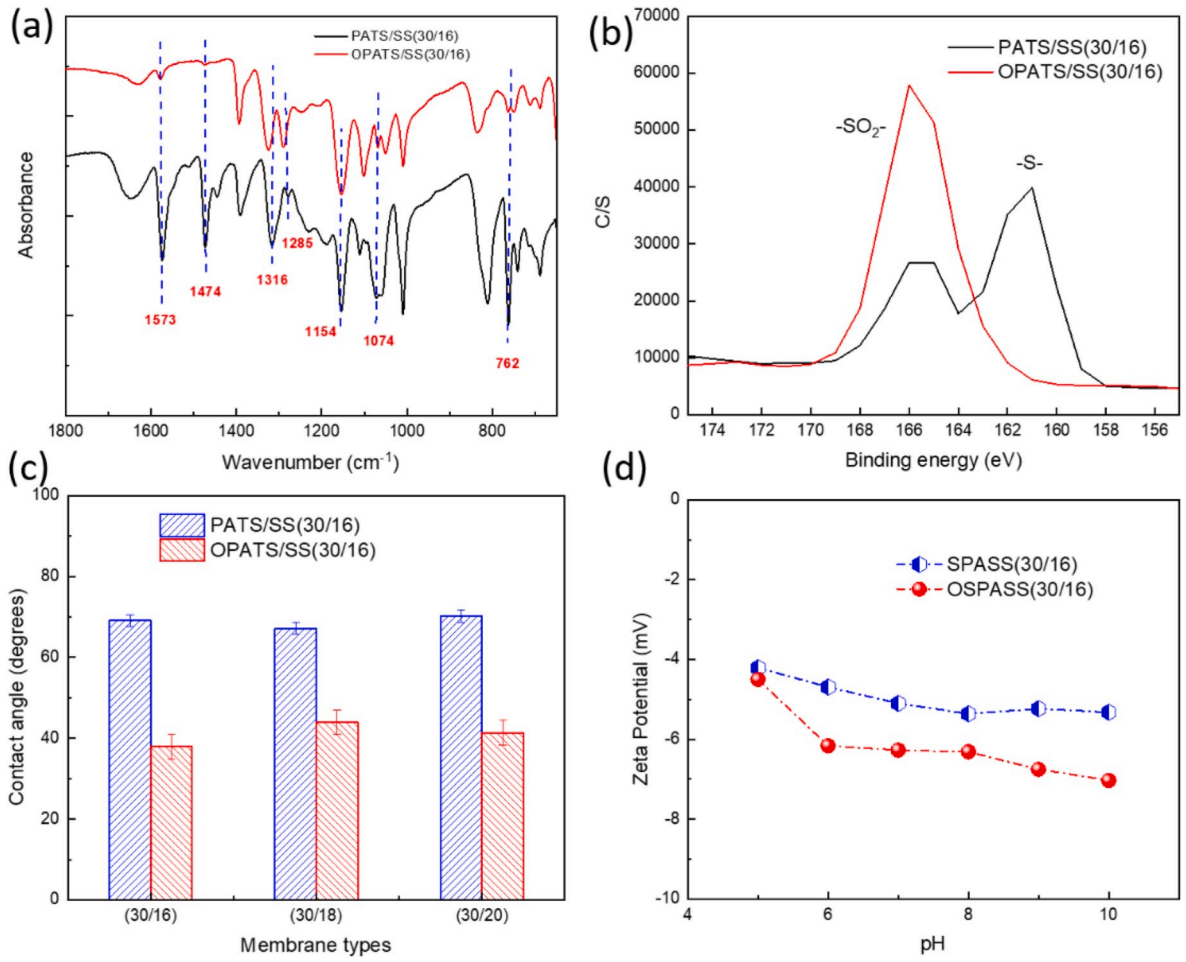

Fig. 7. (a) FT-IR spectrum of PATS/SS and OPATS/SS membranes; (b) XPS spectra of PATS/SS and after oxidation (OPATS/SS); (c) water contact angle of PATS/SS and OPATS/SS membranes; (d) zeta potential of PATS/SS and OPATS/SS membrane at various pH values.

surface, as more PATS/SS material comes in and repairs the valley area. The increase in roughness is mainly caused by the swelling of PATS/SS in acetic acid. During the oxidation treatment, the acetic acid molecules penetrated into the PATS/SS membrane and caused swelling, which provided channels for hydrogen peroxide molecules to diffuse into the PATS/SS membrane and react with the -S- groups in PATS/SS chains. The nano-sized triangular strips generated on the oxidized PATS/SS membrane surface can be attributed to the relaxation of PATS/SS chains during swelling and the reconfiguration of the OPATS/SS chains arrangement.

The solvent resistance of PATS/SS and OPATS/SS membranes was investigated by immersing them in NMP solution (Fig. 6). Photos were taken at 0 min, 1 min, 10 min and 24 h. The PATS/SS membrane is immediately dissolved in NMP for 10 min; the OPATS/SS membrane was found to be not dissolved, still retaining its structure even after 24 h. To shed light on the mechanism for the solvent resistant improvement, the chemical structure of PATS/SS and OPATS/SS was characterized by FT-IR. As shown in Fig. 7a, the peaks at 1074 cm^{-1} and 762 cm^{-1} attributed to -S- groups almost completely disappeared after oxidation, while the characteristic peak at 1285 cm^{-1} corresponding to the $–SO_2$- groups becomes larger, indicating that -S- groups were oxidized to $–SO_2$- groups. The adsorption bands appearing at 1573 and 1474 cm^{-1} attributed to the stretching vibration of benzene rings disappeared after oxidation. This is mainly because the structure attached on both sides of the benzene rings are exactly the same, giving a perfect symmetry after oxidation when -S- becomes $–SO_2$- [24]. The change of chemical composition during the oxidation process was further examined by XPS. As shown in Fig. 7b, after oxidation, the sulfur peak at 161.0 eV responding to -S- in the polymer backbone disappeared after the oxidation, while the intensity of the peak at 166.0 eV attributed to the $–SO_2$- group increases [24,45]. In addition, the peak area of $–SO_2$- in OPATS/SS is the sum of the -S- and $–SO_2$- peak areas in the PATS/SS spectrum. This suggests that the -S- was changed to $–SO_2$- groups after oxidization, which confirms the analysis of the FT-IR results. Compared with the $–SO_2$- bond, the -S- bond length is longer and bond angle is larger, which makes the PATS/SS molecular chain easier to move. The oxidation treatment converts the -S- bond to a $–SO_2$- bond, thereby increasing the rigidity and intermolecular forces of the polymer chains [24,46]. These factors give the OPATS/SS membrane an excellent chemical stability in NMP. Due to the enhanced solvent resistance of OPATS/SS, this membrane is promising to be used in organic solvent nanofiltration.

The water contact angle of PASS and OPATS/SS membranes is shown in Fig. 7c. The concentration of the casting solution has little effect on the water contact angle. However, oxidation treatment reduced the contact angle from 69.1° (PATS/SS membrane) to 37.9° (OPATS/SS membrane), indicating a significant improvement in hydrophilicity. It is well known that the hydrophilicity of a membrane is mainly determined by the surface roughness and the polarity of the membrane materials [47,48]. According to the results of FT-IR and XPS, the increase of polar $–SO_2$- in the OPATS/SS molecular chain after oxidation reaction is the main reason for the decrease of the water contact angle. In addition, AFM results show an increase in the roughness of the OPATS/SS membrane, which is also helpful for improving the hydrophilicity.

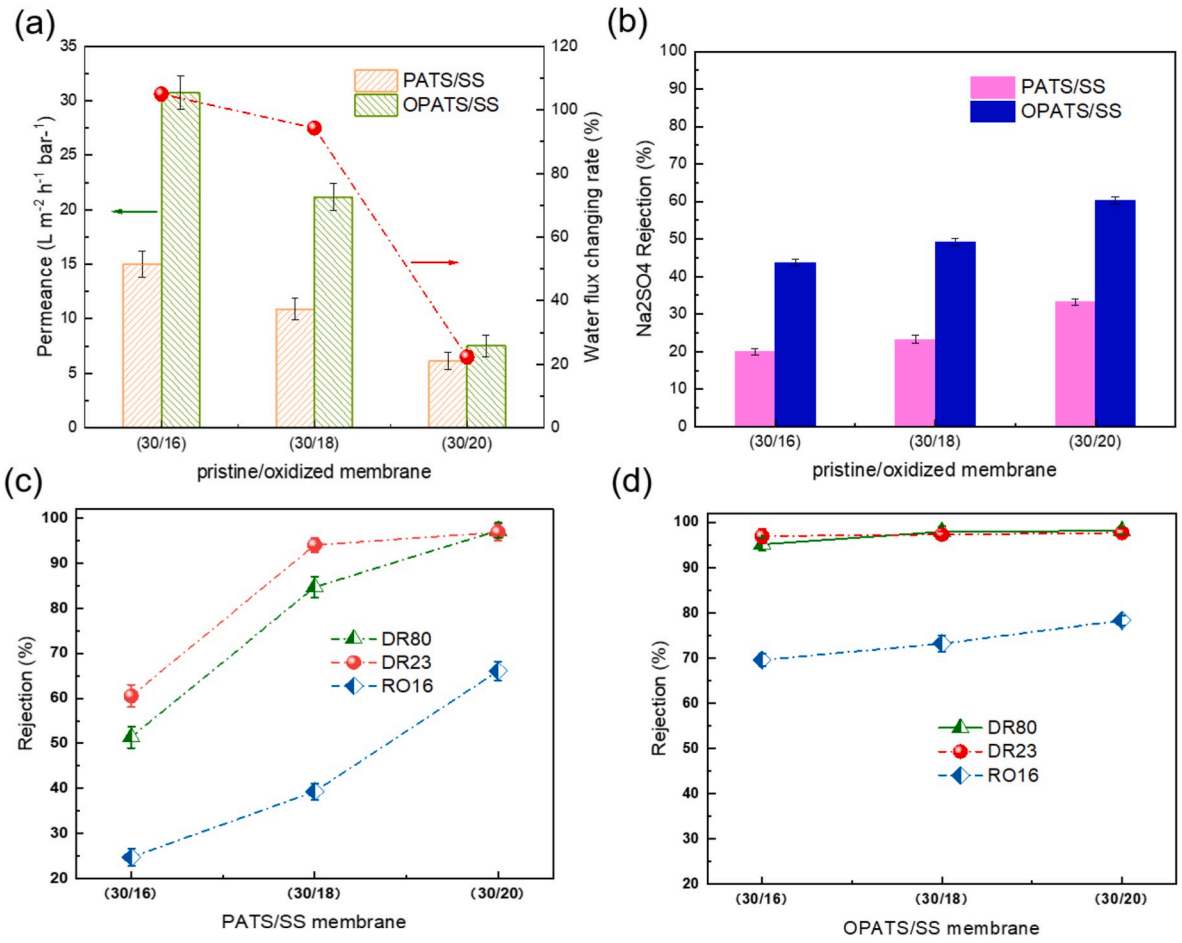

Fig. 8. The effect of oxidation treatment and casting solution concentration on membrane performance. (a) water permeability of PATS/SS and OPATS/SS membranes; (b) salt rejection of PATS/SS and OPATS/SS membranes; (c) dye retention of PATS/SS membrane; (d) dye retention of OPATS/SS membrane. The influent dye concentration used was of 0.5 g L^{-1}. Pressures applied were 6 bar.

Hydrophilic properties can help the membrane to reduce fouling effects, and to increase the membrane permeability.

The zeta potential of PATS/SS and OPATS/SS membranes was measured at different solution pH (4–9); the effect of oxidation treatment on the surface charge of the membrane was investigated (Fig. 7d). The primeval PATS/SS membrane is negatively charged, as illustrated in Fig. 7d. After oxidization, the OPATS/SS membrane showed an enhanced negative zeta potential at all solution pH values investigated. Oxidative treatment can increase the membrane charge by increasing dissociation of sulfonate groups due to the strong electronegative of oxygen in the $–SO_2-$ groups [49]. In addition, compared to -S- groups, $–SO_2-$ groups are more negative groups. During the oxidization, the -S- groups was changed to $–SO_2-$ groups, thus, the surface of the membrane becomes more negative charged after oxidization. It is well known that the zeta potential has a great influence on the rejection characteristics of charged membranes [50]. Therefore, the electrostatic interaction between negatively charged dyes and OPATS/SS surface groups may also play an important role in negatively charged dyes solution [51,52].

3.3. Nanofiltration performance of PATS/SS and OPATS/SS membranes

3.3.1. Membrane molecular weight cut off (MWCO)

The effective pore size of membranes was obtained from the MWCOs, which were determined by the molecular weight of the PEG aqueous solute in which rejection is equal to 90%. Fig. S3 exhibits the rejection curves of the tested membranes to PEG with different molecular weights. The MWCO of the membrane is 1168 and 1402 g mol^{-1} for the tested PATS/SS and OPATS/SS respectively, showing a decreasing tendency with oxidation treatment. In addition, the calculated mean pore size of the membrane was 0.86 and 0.95 nm (Table S3), respectively. Compared to the pristine membrane, the smaller pore size of the oxidized membrane is likely due to the formation of a membrane with a higher packing density and intermolecular interaction as the result of oxidation treatment. The bond length and bond angle of the C–S bond are 180 p.m. and 90°, which is relatively large, giving more freedom for the PATS/SS chain to move, while the $–SO_2-$ units enable the PATS/SS to have a more rigid chain because the polar groups would reinforce the intermolecular interaction of the polymer chains. In addition, the $–SO_2-$ units occupies a larger physical space than -S-. The oxidation treatment converts the -S- bond to a $–SO_2-$ bond, increasing the packing density, rigidity and intermolecular forces of the polymer chains [24,46]. The reduction of the pore size will have a beneficial effect on the improvement of the selectivity of the NF membrane.

It is interesting to take note that the oxidation treatment made the membrane pores smaller, but the porosity increased. Oxidation treatment increased the porosity of the pristine PATS/SS (30/16) membrane by 81.32%–84.43% (Table S3). This oxidation treatment results in a higher porosity since polymer swelling in the acetic acid solution causes the PATS/SS molecular chain to change from a compacted state to a relaxed state to increase the porosity [15,24,53].

3.3.2. Permeation and rejection

The selectivity of a nanofiltration membrane is mainly determined by size exclusion, the Donnan effect and the dielectric effect [16,17,19,

20]. The Donnan effect is essentially electrostatic repulsion, so it is closely related to the charges of both the membrane surface and the solute. A series of negatively charged dyes (DR80, DR23 and RO16) was employed to investigate the performance of PATS/SS and OPATS/SS nanofiltration membranes. In addition, a feed solution containing Na_2SO_4 was also used to test the inorganic salt rejection performance, thereby judging the application potential of membrane in fractionation of dye/salt mixtures.

Fig. 8 shows the permeance, and the rejections dyes and Na_2SO_4 of the pristine and oxidized PATS/SS membrane. Oxidation treatment can effectively improve the permeance of a membrane, as illustrated in Fig. 8a. For instance, compared with the PATS/SS (30/16) membrane, the OPATS/SS (30/16) membrane can yield a 105% improvement of the permeance (from 15.00 L m^{-2} h^{-1} bar^{-1} to 30.75 L m^{-2} h^{-1} bar^{-1}). The increase of permeance was mainly caused by the enhanced membrane hydrophilicity, permeable area and porosity; this was confirmed by the contact angle results, SEM images and membrane porosity discussed above. Although the oxidation treatment will make the pore size smaller and negatively affect the permeability, the permeability increase caused by the enhanced porosity will cover up the negative effect of the former. The enhanced hydrophilicity of the PATS/SS membrane was ascribed to the increasing number of $–SO_2$- bonds in the OPATS/SS membrane chain, the improved membrane surface area was due to the wave structure, triangular strips and volcanic structure on the membrane, while enhanced membrane porosity was caused by the relaxation of polymer chains during swelling in the oxidized solution. These features synergistically contribute to the enhancement of rejection and permeability of OPATS/SS after oxidization. The increase in the concentration of the casting solution causes the membrane to be dense, resulting in a decrease of the membrane permeability and an increase in selectivity. The oxidation can increase the permeability (Fig. 8a) and selectivity (Fig. 8b, c and d) simultaneously, but the oxidation enhancement effect of the low concentration casting solution is more obvious.

Fig. S5 and Table S5 compares the simultaneous improvement of permeability and selectivity for nanofiltration of dye solutions between this study and the literature. Considering the simultaneous improvement of permeability and selectivity (breaking balance between permeability and selectivity), the performance promotion of modified membranes compared with the nascent one was evaluated [54,55]. Obviously, the oxidized PATS/SS membrane fabricated by this molecular design method stood out, with a significantly improved NF performance. Most studies aim at improving the selectivity while sacrificing permeability, due to the balance between permeability and selectivity, which is the bottleneck of nanofiltration development [6–8]. However, in this study, the OPATS/SS membrane (16 wt%) was shown to have an enhancement of rejection and permeability simultaneously. This is a rare phenomenon that breaks the balance. The pristine PATS/SS (30/16) membrane exhibits rejections lower than 60% for dyes (60.53% for DR23, 51.37% for DR80, and 24.72% for RO16) and 20% rejection for Na_2SO_4, indicating that the rejection performance of the PATS/SS (30/16) membrane is not excellent (Fig. 8b and c). In contrast, the oxidized PATS/SS membranes show a significantly higher selectivity; the OPATS/SS (30/16) membrane shows the dyes rejection decrease in order of DR23 (96.99%)> DR80 (95.13%)> RO16 (69.61%) and Na_2SO_4 rejection of 43.77%, indicating that the rejection performance of the OPATS/SS (30/16) membrane is greatly improved (Fig. 8b, d). For instance, compared with the PATS/SS (30/16) membrane, the OPATS/SS (30/16) membrane can yield an 85.2% improvement of the DR80 rejection (from 51.37% to 95.13% rejection). Based on the zeta potential results, the OPATS/SS membrane is more negatively charged compared with the pristine PATS/SS membrane. Accordingly, this result should be attributed to the enhanced repulsion force between DR80 molecules (negatively charged) and the oxidized PATS/SS membrane, which will more strongly repel DR80 molecules, thereby increasing the DR80 rejection [15,24,53]. As shown in Fig. S3 and Table S3, the mean pore size of the pristine PATS/SS (30/16) membrane is 0.95 nm and the mean pore size of

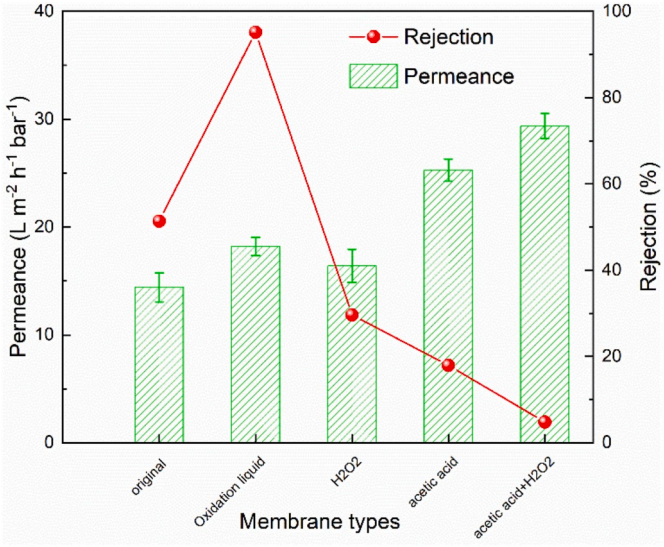

Fig. 9. oxidation reason analysis based on PATS/SS (30/16) membrane. (DR80 dye solution).

OPATS/SS (30/16) membrane is 0.86 nm, which means that the oxidation treatment also enhances the size exclusion effect to achieve the purpose of improving rejection.

The increase of permeation is also attributed to the swelling of PATS/SS in the acetic acid solution. It causes the PATS/SS molecular chain to change from a compacted state to a relaxed state. Furthermore, the immersion of acetic acid solution into the molecular chains creates more channels, thus the permeation can be increased.

Fig. S4 shows images of the pristine and oxidized PATS/SS membrane before and after nanofiltration of a dye solution. As shown in Fig. S4, the color of the oxidized PATS/SS membrane is lighter, due to the change in chemical structure during the oxidation treatment. After filtration, it can be observed that the pristine PATS/SS membrane surface is covered with a relatively thick dye layer, while the oxidized PATS/SS membrane is only slightly polluted (Figs. S4a and b). The enhanced antifouling ability of the oxidized PATS/SS membrane is attributed to the improvement in surface hydrophilicity and negative charge. Obviously, the hydrophilicity of the OPATS/SS membrane would be greatly enhanced by oxidation treatment, resulting in strong hydration (hydration layer), which effectively inhibits the binding of the dye to the membrane surface. The negative charge of the OPATS/SS membrane is enhanced after oxidation, which could enhance the repulsion force between negatively charged dye molecules and the OPATS/SS membrane surface and further prevent membrane fouling. In addition, the oxidation treatment makes the effective mean pore size of the membrane smaller, and it is difficult for dye molecules to invade the membrane body, so the reduction of effective mean pore size can also play an important role in improving the antifouling performance.

In order to further explain the oxidation principle, the OPATS/SS (30/16) membrane was chosen in the following experiment. Furthermore, the sulfonation degree may also affect the performance of the membrane in nanofiltration.

3.3.3. *The role of chemicals in oxidation solution during oxidization*

As mentioned above, oxidation treatment (hydrophilicity, permeable area, negatively charged surface) and a slight swelling (narrow pore size, more channels) can increase both the permeability and selectivity of membrane. Fig. 9 shows the DR80 dye solution nanofiltration performance of the PATS/SS (30/16) membrane treated with different solutions (oxidation solution (3 v% H_2SO_4 + 87 v% acetic acid + 10 v% H_2O_2), H_2O_2, acetic acid, 90 v% acetic acid + 10 v% H_2O_2). After treatment of the PATS/SS (30/16) membranes with acetic acid and

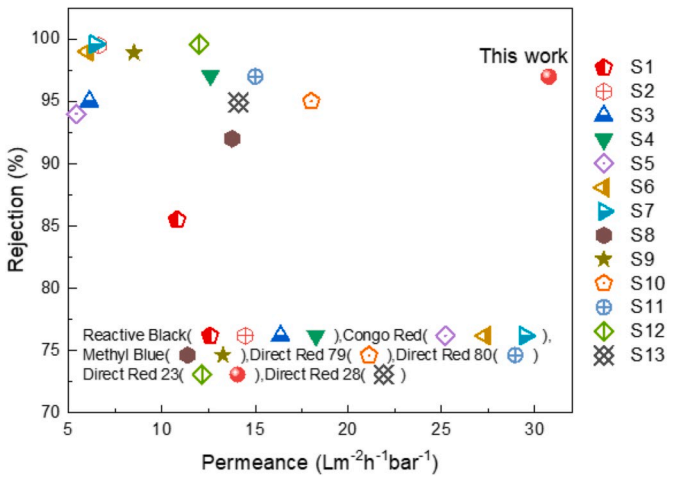

Fig. 10. Comparison of the oxidized PATS/SS membrane with various commercial and lab-made NF membrane reported for dye desalination (for details see Table S4).

acetic acid + H_2O_2, the permeation increased sharply and the rejection decreased significantly, indicating that the swelling was too strong. In addition, H_2O_2 is relatively mild, and the permeation of the PATS/SS membrane treated with H_2O_2 is slightly increased by a relatively small decrease in rejection. It was found that the permeation and rejection of the membrane can be simultaneously increased under the treatment of oxidation solution. It can be found that the H_2SO_4 is an indispensable catalyst in the oxidation treatment, which is why only strong swelling (membrane treated by acetic acid + H_2O_2) occurs without the H_2SO_4.

In order to highlight the performance of the OPATS/SS membrane, the separation performance of various membranes was compared (Fig. 10). The OPATS/SS membrane shows the highest water permeability, with a relatively high dye rejection. Despite satisfactory rejections, most membranes have a relative low water permeance, i.e., below 15 $Lm^{-2}h^{-1}bar^{-1}$. The water permeances through our OPATS/SS membrane were nearly 2–6 times higher than the permeances reported for other lab-made NF membranes (see Table S4). This is likely due to the combination of a high porosity, high permeable area and strong hydrophilicity. More importantly, this work provides an efficient molecular design method to significantly improve performance. The OPATS/SS membrane was shown to have an enhancement of rejection and permeability simultaneously. This is a rare phenomenon that breaks the balance between permeability and selectivity. These results indicate that the OPATS/SS membrane is competitive in dye desalination.

4. Conclusions

A novel strategy to achieve an enhancement of permeability and selectivity by increasing the membrane porosity, effective area, hydrophilicity, surface electrical charge, and decreasing pore size was proposed in this study. More specifically, oxidation converts the -S- bonds in PATS/SS into $–SO_2-$ bonds, which improve the negative charge, hydrophilicity, permeable area, and swelling resistance of OPATS/SS. Most importantly, the OPATS/SS membrane has an improved permeance and rejection at the same time during nanofiltration of dye solutions (For example, 105% improvement for permeance and 85.2% improvement for rejection performance of DR80 dye solution nanofiltration), significantly breaking through the balance between permeability and selectivity. In addition, the oxidized PATS/SS membrane allowed for fractionation of dye/salt, antifouling and organic solvent resistance ability.

Declaration of competing interest

The authors declare that they have no known competing financial interests or personal relationships that could have appeared to influence the work reported in this paper.

CRediT authorship contribution statement

Pengrui Jin: Conceptualization, Methodology, Validation, Formal analysis, Investigation, Writing - original draft, Writing - review & editing. **Shushan Yuan:** Conceptualization, Methodology, Formal analysis, Resources, Writing - review & editing. **Gang Zhang:** Conceptualization, Resources, Writing - original draft. **Junyong Zhu:** Methodology, Formal analysis. **Junfeng Zheng:** Methodology, Formal analysis. **Patricia Luis:** Writing - review & editing. **Bart Van der Bruggen:** Writing - review & editing, Resources, Supervision, Project administration.

Acknowledgements

Pengrui Jin would like to acknowledge the support provided by China Scholarship Council (CSC) of the Ministry of Education, P.R. China (CSC No. 201806050043). The authors are grateful to National Nature Science Foundation of China (NSFC-21304060), the department of science and technology of Jiangsu province for the financial support of this project (BE2019008-4) and the Fundamental Research Funds for the Central Universities. Finally, Pengrui Jin specifically wants to thank the ongoing and unwavering support received from Weiyuan Gao, I love you!

Appendix A. Supplementary data

Supplementary data to this article can be found online at https://doi.org/10.1016/j.memsci.2020.118241.

References

[1] H. Fan, J. Gu, H. Meng, A. Knebel, J. Caro, High-flux membranes based on the covalent organic framework COF-LZU1 for selective dye separation by nanofiltration, Angew. Chem. Int. Ed. 57 (2018) 4083–4087.
[2] Y. Zhan, X. Wan, S. He, Q. Yang, Y. He, Design of durable and efficient poly (arylene ether nitrile)/bioinspired polydopamine coated graphene oxide nanofibrous composite membrane for anionic dyes separation, Chem. Eng. J. 333 (2018) 132–145.
[3] S. Karan, Z. Jiang, A.G. Livingston, Sub–10 nm polyamide nanofilms with ultrafast solvent transport for molecular separation, Science 348 (2015) 1347–1351.
[4] J. Lin, C.Y. Tang, W. Ye, S.-P. Sun, S.H. Hamdan, A. Volodin, C. Van Haesendonck, A. Sotto, P. Luis, B. Van der Bruggen, Unraveling flux behavior of superhydrophilic loose nanofiltration membranes during textile wastewater treatment, J. Membr. Sci. 493 (2015) 690–702.
[5] S. Wang, D. Mahalingam, B. Sutisna, S.P. Nunes, 2D-dual-spacing channel membranes for high performance organic solvent nanofiltration, J. Mater. Chem. 7 (2019) 11673–11682.
[6] H.B. Park, J. Kamcev, L.M. Robeson, M. Elimelech, B.D. Freeman, Maximizing the right stuff: the trade-off between membrane permeability and selectivity, Science (2017) 356, eaab0530.
[7] Y. Zhang, W. Yu, R. Li, Y. Xu, L. Shen, H. Lin, B.-Q. Liao, G. Wu, Novel conductive membranes breaking through the selectivity-permeability trade-off for Congo red removal, Separ. Purif. Technol. 211 (2019) 368–376.
[8] X. Wu, L. Hao, J. Zhang, X. Zhang, J. Wang, J. Liu, Polymer-Ti3C2Tx composite membranes to overcome the trade-off in solvent resistant nanofiltration for alcohol-based system, J. Membr. Sci. 515 (2016) 175–188.
[9] J.R. Werber, C.O. Osuji, M. Elimelech, Materials for next-generation desalination and water purification membranes, Nature Reviews Materials 1 (2016) 16018.
[10] X. Li, S. Chou, R. Wang, L. Shi, W. Fang, G. Chaitra, C.Y. Tang, J. Torres, X. Hu, A. G. Fane, Nature gives the best solution for desalination: aquaporin-based hollow fiber composite membrane with superior performance, J. Membr. Sci. 494 (2015) 68–77.
[11] H. Yu, X. Qiu, N. Moreno, Z. Ma, V.M. Calo, S.P. Nunes, K.-V. Peinemann, Self-assembled asymmetric block copolymer membranes: bridging the gap from ultra- to nanofiltration, Angew. Chem. Int. Ed. 54 (2015) 13937–13941.
[12] X. Qiu, H. Yu, M. Karunakaran, N. Pradeep, S.P. Nunes, K.-V. Peinemann, Selective separation of similarly sized proteins with tunable nanoporous block copolymer membranes, ACS Nano 7 (2013) 768–776.

[13] Y. Meng, L. Shu, L. Liu, Y. Wu, L.-H. Xie, M.-J. Zhao, J.-R. Li, A high-flux mixed matrix nanofiltration membrane with highly water-dispersible MOF crystallites as filler, J. Membr. Sci. (2019) 117360.
[14] R.P. Pandey, K. Rasool, V.E. Madhavan, B. Aïssa, Y. Gogotsi, K.A. Mahmoud, Ultrahigh-flux and fouling-resistant membranes based on layered silver/MXene (Ti 3 C 2 T x) nanosheets, J. Mater. Chem. 6 (2018) 3522–3533.
[15] J. Wang, R. He, X. Han, D. Jiao, J. Zhu, F. Lai, X. Liu, J. Liu, Y. Zhang, B. Van der Bruggen, High performance loose nanofiltration membranes obtained by a catechol-based route for efficient dye/salt separation, Chem. Eng. J. (2019) 121982.
[16] F.G. Donnan, Theory of membrane equilibria and membrane potentials in the presence of non-dialysing electrolytes. A contribution to physical-chemical physiology, J. Membr. Sci. 100 (1995) 45–55.
[17] W. Deen, Hindered transport of large molecules in liquid-filled pores, AIChE J. 33 (1987) 1409–1425.
[18] A.W. Mohammad, Y. Teow, W. Ang, Y. Chung, D. Oatley-Radcliffe, N. Hilal, Nanofiltration membranes review: recent advances and future prospects, Desalination 356 (2015) 226–254.
[19] Y. Zhu, H. Zhu, G. Li, Z. Mai, Y. Gu, The effect of dielectric exclusion on the rejection performance of inhomogeneously charged polyamide nanofiltration membranes, J. Nanoparticle Res. 21 (2019) 217.
[20] S. Bandini, D. Vezzani, Nanofiltration modeling: the role of dielectric exclusion in membrane characterization, Chem. Eng. Sci. 58 (2003) 3303–3326.
[21] G. Zeng, Z. Ye, Y. He, X. Yang, J. Ma, H. Shi, Z. Feng, Application of dopamine-modified halloysite nanotubes/PVDF blend membranes for direct dyes removal from wastewater, Chem. Eng. J. 323 (2017) 572–583.
[22] G. Zhang, S. Yuan, S. Cao, G. Yan, X. Wang, J. Yang, B. Van der Bruggen, Functionalized poly (arylene ether sulfone) containing hydroxyl units for the fabrication of durable, superhydrophobic oil/water separation membranes, Nanoscale 11 (2019) 7166–7175.
[23] A.A. Tashvigh, L. Luo, T.-S. Chung, M. Weber, C. Maletzko, A novel ionically cross-linked sulfonated polyphenylsulfone (sPPSU) membrane for organic solvent nanofiltration (OSN), J. Membr. Sci. 545 (2018) 221–228.
[24] S. Yuan, J. Wang, X. Li, J. Zhu, A. Volodine, X. Wang, J. Yang, P. Van Puyvelde, B. Van der Bruggen, New promising polymer for organic solvent nanofiltration: oxidized poly (arylene sulfide sulfone), J. Membr. Sci. 549 (2018) 438–445.
[25] D. Li, Z. Li, F. Hu, S. Long, G. Zhang, J. Yang, Pendant crosslinked poly (aryl ether sulfone) copolymers sulfonated on backbone for proton exchange membranes, Polym. Eng. Sci. 54 (2014) 2013–2022.
[26] J. Pang, K. Shen, D. Ren, S. Feng, Z. Jiang, Polyelectrolyte based on tetra-sulfonated poly (arylene ether) s for direct methanol fuel cell, J. Power Sources 226 (2013) 179–185.
[27] N. Widjojo, T.-S. Chung, M. Weber, C. Maletzko, V. Warzelhan, The role of sulphonated polymer and macrovoid-free structure in the support layer for thin-film composite (TFC) forward osmosis (FO) membranes, J. Membr. Sci. 383 (2011) 214–223.
[28] A.D. Sabde, M.K. Trivedi, V. Ramachandhran, M.S. Hanra, B.M. Misra, Casting and characterization of cellulose acetate butyrate based UF membranes, Desalination 114 (1997) 223–232.
[29] X. Liu, H. Liu, P. Li, Effect of polymer dope concentration on the morphology and performance of PES/PDMS hollow fiber composite membrane for gas separation, PES 500 (2017) 72.
[30] K.C. Khulbe, T. Matsuura, S.H. Noh, Effect of thickness of the PPO membranes on the surface morphology, J. Membr. Sci. 145 (1998) 243–251.
[31] Z. Huang, W. Hong, Z. Suo, Nonlinear analyses of wrinkles in a film bonded to a compliant substrate, J. Mech. Phys. Solid. 53 (2005) 2101–2118.
[32] J.-F. Blanco, J. Sublet, Q.T. Nguyen, P. Schaetzel, Formation and morphology studies of different polysulfones-based membranes made by wet phase inversion process, J. Membr. Sci. 283 (2006) 27–37.
[33] N. Widjojo, T.-S. Chung, M. Weber, C. Maletzko, V. Warzelhan, The role of sulphonated polymer and macrovoid-free structure in the support layer for thin-film composite (TFC) forward osmosis (FO) membranes, J. Membr. Sci. 383 (2011) 214–223.
[34] S. Sahebi, S. Phuntsho, Y.C. Woo, M.J. Park, L.D. Tijing, S. Hong, H.K. Shon, Effect of sulphonated polyethersulfone substrate for thin film composite forward osmosis membrane, Desalination 389 (2016) 129–136.
[35] N. Widjojo, T.-S. Chung, M. Weber, C. Maletzko, V. Warzelhan, A sulfonated polyphenylenesulfone (sPPSU) as the supporting substrate in thin film composite (TFC) membranes with enhanced performance for forward osmosis (FO), Chem. Eng. J. 220 (2013) 15–23.
[36] G. Han, B. Zhao, F. Fu, T.-S. Chung, M. Weber, C. Staudt, C. Maletzko, High performance thin-film composite membranes with mesh-reinforced hydrophilic sulfonated polyphenylenesulfone (sPPSU) substrates for osmotically driven processes, J. Membr. Sci. 502 (2016) 84–93.
[37] G. Han, T.-S. Chung, M. Toriida, S. Tamai, Thin-film composite forward osmosis membranes with novel hydrophilic supports for desalination, J. Membr. Sci. 423 (2012) 543–555.
[38] J. Wijmans, J. Kant, M. Mulder, C. Smolders, Phase separation phenomena in solutions of polysulfone in mixtures of a solvent and a nonsolvent: relationship with membrane formation, Polymer 26 (1985) 1539–1545.
[39] L. Xu, F. Qiu, Simultaneous determination of three Flory–Huggins interaction parameters in polymer/solvent/nonsolvent systems by viscosity and cloud point measurements, Polymer 55 (2014) 6795–6802.
[40] S. Shilton, G. Bell, J. Ferguson, The rheology of fibre spinning and the properties of hollow-fibre membranes for gas separation, Polymer 35 (1994) 5327–5335.
[41] N. Peng, N. Widjojo, P. Sukitpaneenit, M.M. Teoh, G.G. Lipscomb, T.-S. Chung, J.-Y. Lai, Evolution of polymeric hollow fibers as sustainable technologies: past, present, and future, Prog. Polym. Sci. 37 (2012) 1401–1424.
[42] Y. Feng, G. Han, L. Zhang, S.-B. Chen, T.-S. Chung, M. Weber, C. Staudt, C. Maletzko, Rheology and phase inversion behavior of polyphenylenesulfone (PPSU) and sulfonated PPSU for membrane formation, Polymer 99 (2016) 72–82.
[43] P.S. Zhong, N. Widjojo, T.-S. Chung, M. Weber, C. Maletzko, Positively charged nanofiltration (NF) membranes via UV grafting on sulfonated polyphenylenesulfone (sPPSU) for effective removal of textile dyes from wastewater, J. Membr. Sci. 417 (2012) 52–60.
[44] Z. Wang, Z. Wang, S. Lin, H. Jin, S. Gao, Y. Zhu, J. Jin, Nanoparticle-templated nanofiltration membranes for ultrahigh performance desalination, Nat. Commun. 9 (2018) 2004.
[45] Y. Liu, A. Bhatnagar, Q. Ji, J. Riffle, J. McGrath, J. Geibel, T. Kashiwagi, Influence of polymerization conditions on the molecular structure stability and physical behavior of poly (phenylene sulfide sulfone) homopolymers, Polymer 41 (2000) 5137–5146.
[46] H.M. Colquhoun, P.L. Aldred, F.H. Kohnke, P.L. Herbertson, I. Baxter, D. J. Williams, Crystal and molecular structures of poly (1, 4-phenylenesulfone) and its trisulfone and tetrasulfone oligomers, Macromolecules 35 (2002) 1685–1690.
[47] B. Bharti, S. Kumar, R. Kumar, Superhydrophilic TiO2 thin film by nanometer scale surface roughness and dangling bonds, Appl. Surf. Sci. 364 (2016) 51–60.
[48] N.J. Shirtcliffe, G. McHale, M.I. Newton, C.C. Perry, P. Roach, Porous materials show superhydrophobic to superhydrophilic switching, Chem. Commun. (2005) 3135–3137.
[49] M.-L. Luo, J.-Q. Zhao, W. Tang, C.-S. Pu, Hydrophilic modification of poly(ether sulfone) ultrafiltration membrane surface by self-assembly of TiO2 nanoparticles, Appl. Surf. Sci. 249 (2005) 76–84.
[50] A.E. Childress, M. Elimelech, Relating nanofiltration membrane performance to membrane charge (electrokinetic) characteristics, Environ. Sci. Technol. 34 (2000) 3710–3716.
[51] S. Xia, L. Yao, Y. Zhao, N. Li, Y. Zheng, Preparation of graphene oxide modified polyamide thin film composite membranes with improved hydrophilicity for natural organic matter removal, Chem. Eng. J. 280 (2015) 720–727.
[52] J. Ma, X. Guo, Y. Ying, D. Liu, C. Zhong, Composite ultrafiltration membrane tailored by MOF@ GO with highly improved water purification performance, Chem. Eng. J. 313 (2017) 890–898.
[53] Y. Li, S. Yuan, C. Zhou, Y. Zhao, B. Van der Bruggen, A high flux organic solvent nanofiltration membrane from Kevlar aramid nanofibers with in situ incorporation of microspheres, J. Mater. Chem. 6 (2018) 22987–22997.
[54] Z. Zhai, N. Zhao, W. Dong, P. Li, H. Sun, Q.J. Niu, In situ assembly of a zeolite imidazolate framework hybrid thin-film nanocomposite membrane with enhanced desalination performance induced by noria–polyethyleneimine codeposition, ACS Appl. Mater. Interfaces 11 (2019) 12871–12879.
[55] T.H. Lee, J.Y. Oh, S.P. Hong, J.M. Lee, S.M. Roh, S.H. Kim, H.B. Park, ZIF-8 particle size effects on reverse osmosis performance of polyamide thin-film nanocomposite membranes: importance of particle deposition, J. Membr. Sci. 570 (2019) 23–33.